Preparation and Characterization of $VO(HPO_4)\cdot 0.5H_2O$ and Its Topotactic Transformation to $(VO)_2P_2O_7$

Jack W. Johnson,* David C. Johnston, Allan J. Jacobson, and John F. Brody

Contribution from the Exxon Research and Engineering Company, Corporate Research-Science Laboratories, Annandale, New Jersey 08801. *Received February 10, 1984*

Abstract: Vanadyl hydrogen phosphate hemihydrate, $VO(HPO_4)\cdot 0.5H_2O$, has been characterized through a combination of techniques including infrared spectroscopy, paper chromatography, X-ray powder diffraction, scanning electron microscopy, thermogravimetric analysis and magnetic susceptibility measurements. It crystallizes in the orthorhombic system, a = 7.434 (2) Å, b = 9.620 (2) Å, c = 5.699 (1) Å in space group $Pmmn$ or $P2_1mn$. The structure consists of two-dimensional layers of HPO_4^{2-} anions and pairs of antiferromagnetically coupled V^{4+} cations. The layers are held together by strong hydrogen bonding. Above ~350 °C, $VO(HPO_4)\cdot 0.5H_2O$ undergoes a topotactic dehydration to $(VO)_2P_2O_7$, an active and selective catalyst for the oxidation of butane to maleic anhydride.

Vanadium phosphorus oxides have a rich and complex chemistry that is, as yet, incompletely explored. Both the vanadium oxidation state and the phosphorus to vanadium ratio can be varied. Even at a P/V ratio restricted to 1, several well-characterized phases are known, listed in order of increasing vanadium oxidation state: VPO_4,[1,2] $(VO)_2P_2O_7$,[1,3-9] α_I-$VOPO_4$,[10-14] α_{II}-$VOPO_4$,[13,15,16] β-$VOPO_4$,[12,17] and $VOPO_4\cdot 2H_2O$.[10-12,14,18-20] The simple C_4 hydrocarbons butane and butene can be oxidized with air to maleic anhydride over vanadium phosphate catalysts.[3,5-7,21-25] The consensus of these studies indicates that the best catalysts have vanadium in the +4 oxidation state and a P/V ratio of approximately 1. The pyrophosphate, $(VO)_2P_2O_7$, is the only well-characterized solid phase that has these values for vanadium oxidation state and P/V ratio and it has been detected by X-ray diffraction in active catalysts which exhibit high selectivities. Catalyst precursors, usually identified as blue or green solids,[3,26-30] must also contain vanadium(IV) monophosphates but these have not been thoroughly characterized even though results of some X-ray, SEM, infrared, and chemical analyses on these precursors have been reported.[25,26,29-32]

During earlier studies directed toward the synthesis of solid materials with layered structures composed of alternating inorganic and organic layers,[33,34] we investigated the reactions of the vanadium phosphate $VOPO_4$ and its hydrates with neutral organic donor ligands such as pyridine.[35] Coordination intercalation compounds in which the pyridine molecules were directly bound to vanadium in the $VOPO_4$ layers were synthesized but under some conditions reduction of V^{5+} to V^{4+} along with oxidative coupling of the organic ligand was observed. This redox chemistry of $VOPO_4\cdot 2H_2O$ was studied in detail by using two different approaches. First, $VOPO_4\cdot 2H_2O$ was reduced in aqueous suspension with mild inorganic reducing agents. These reactions led to intercalation compounds $A_xVOPO_4\cdot nH_2O$, where A is a mono- or divalent cation, in which the structural arrangement of the $VOPO_4$ layers had been retained.[36] Second, $VOPO_4\cdot 2H_2O$ was reacted with a variety of organic compounds to study the fate of the vanadium phosphate when reduced in a more complicated process. The reactions led not to intercalation but to the formation of a new layer structure vanadium(IV) hydrogen phosphate, $VO(HPO_4)\cdot 0.5H_2O$, which is related to the catalysis used to produce maleic anhydride from butene or butane.[3-7,21-32,37-41]

In this paper we describe methods for the preparation of $VO(HPO_4)\cdot 0.5H_2O$, its structural, spectroscopic, and magnetic properties, and its thermal transformation to vanadyl pyrophosphate, $(VO)_2P_2O_7$.

Synthesis and Characterization of Vanadium(IV) Hydrogen Phosphate Hemihydrate. The results of exploratory experiments

(1) Tudo, J.; Carton, D. *C. R. Hebd. Seances Acad. Sci., Ser. C* **1979**, *289*, 219–221.
(2) Ladwig, G. *Z. Chem.* **1979**, *19*, 386.
(3) Seeboth, H.; Freiberg, H.-J.; Hopf, G.; Kreissig, J.; Kubias, B.; Ladwig, G.; Lücke, B.; Müller, G.; Wolf, H. DDR Patent 113 210, 1975.
(4) Schneider, R. A. U.S. Patent 3 864 280, 1975.
(5) Seeboth, H.; Kubias, B.; Wolf, H.; Lücke, B. *Chem. Techn.* **1976**, *28*, 730–734.
(6) Seeboth, H.; Ladwig, G.; Kubias, B.; Wolf, G.; Lücke, B. *Ukr. Khim. Zh.* **1977**, *43*, 842–844.
(7) Bordes, E.; Courtine, P. *J. Catal.* **1979**, *57*, 236–252.
(8) Pulvin, S.; Ronis, M.; Courtine, P. *C. R. Hebd. Seances Acad. Sci., Ser. C* **1976**, *283*, 585–587.
(9) Gorbunova, Yu. E.; Linde, S. A. *Dokl. Akad. Nauk SSSR* **1979**, *245*, 584–588.
(10) Ladwig, G. *Z. Anorg. Allg. Chem.* **1965**, *338*, 266–278.
(11) Bordes, E.; Courtine, P. *C. R. Hebd. Seances Acad. Sci., Ser. C* **1972**, *274*, 1375–1377.
(12) Bordes, E.; Courtine, P.; Pannetier, G. *Ann. Chim.* **1973**, *8*, 105–113.
(13) Tachez, M.; Theobald, F.; Bordes, E. *J. Solid State Chem.* **1981**, *40*, 280–283.
(14) Ballutaud, D.; Bordes, E.; Courtine, P. *Mater. Res. Bull.* **1982**, *17*, 519–526.
(15) Jordan, B.; Calvo, C. *Can. J. Chem.* **1973**, *51*, 2621–2625.
(16) Jordan, B. D.; Calvo, C. *Acta Crystallogr., Sect. B* **1976**, *B32*, 2899–2900.
(17) Gopal, R.; Calvo, C. *J. Solid State Chem.* **1972**, *5*, 432–435.
(18) Tietze, H. *Aust. J. Chem.* **1981**, *34*, 2035–2038.
(19) Tachez, M.; Theobald, F.; Bernard, J.; Hewat, A. W. *Rev. Chim. Miner.* **1982**, *19*, 291–300.
(20) Chernorukov, N. G. *Izv. Akad. Nauk SSSR, Neorg. Mater.* **1981**, *17*, 338–341.
(21) Wustneck, N.; Wolf, H.; Seeboth, H. *React. Kinet. Catal. Lett.* **1982**, *21*, 497–503.
(22) Wolf, H.; Wustneck, N.; Seeboth, H.; Belousov, V. M.; Zazigalov, V. A. *Z. Chem.* **1982**, *22*, 193–194.
(23) Hodnett, B. K.; Delmon, B. *J. Chem. Soc., Chem. Commun.* **1983**, 373–374; *Appl. Catal.* **1983**, *6*, 245–259.
(24) Hodnett, B. K.; Permanne, P.; Delmon, B. *Appl. Catal.* **1983**, *6*, 231–244.
(25) Vartuli, J. C.; Zehner, L. R., U.S. Patent 4 247 419, 1981.
(26) (a) Yang, T. C.; Rao, K. K.; Huang, I., U.S. Patent 4 392 986, 1983. (b) Milberger, E. C.; Bremer, N. J.; Dria, D. E., U.S. Patent 4 333 853, 1982; U.S. Patent 4 350 639, 1982.
(27) Morselli, L.; Riva, A.; Trifiro, F.; Zucchi, M.; Emig. G. *Chim. Ind. (Milan)* **1978**, *10*, 791–798.
(28) Martini, G.; Morselli, L.; Riva, A.; Trifiro, F. *React. Kinet. Catal. Lett.* **1978**, *8*, 431–435.
(29) Poli, G.; Resta, I.; Ruggeri, O.; Trifiro, F. *Appl. Catal.* **1981**, *1*, 395–404.
(30) Lanzarini, G.; Trifiro, F.; Ruggeri, O. *Ann. Chim.* **1981**, *71*, 461–468.
(31) Stefani, G.; Fontana, P. U.S. Patent 4 100 106, 1978.
(32) Katsumoto, K. U.S. Patent 4 132 670, 1979.
(33) Johnson, J. W.; Jacobson, A. J.; Rich, S. M.; Brody, J. F. *J. Am. Chem. Soc.* **1981**, *103*, 5246–5247.
(34) Johnson, J. W.; Jacobson, A. J.; Rich, S. M.; Brody, J. F. *Rev. Chem. Miner.* **1982**, *19*, 420–431.
(35) Johnson, J. W.; Jacobson, A. J.; Rich, S. M.; Brody, J. F. *Inorg. Chem.* **1982**, *21*, 3820–3825.
(36) Johnson, J. W.; Jacobson, A. J. *Angew. Chem.* **1983**, *95*, 422; *Angew. Chem., Int. Ed. Engl.* **1983**, *22*, 412–413.
(37) Ai, M. *Bull. Chem. Soc. Jpn.* **1970**, *43*, 3490–3495.
(38) Nakamura, M.; Kawai, K.; Fujiwara, Y. *J. Catal.* **1974**, *34*, 345–355.
(39) Rozhkova, E. V.; Gerei, S. V.; Gorokhovatskii, Ya. B. *Kinet. Katal.* **1974**, *15*, 694–699.
(40) Fricke, R.; Jerschkewitz, H.-G.; Lischke, G.; Öhlman, G. *Z. Anorg. Allg. Chem.* **1979**, *448*, 23–34.
(41) Martini, G.; Trifiro, F.; Vaccari, A. *J. Phys. Chem.* **1982**, *86*, 1573–1576.

0002-7863/84/1506-8123$01.50/0

using $VOPO_4 \cdot 2H_2O$ as an oxidizing agent for organic compounds showed that 2-propanol could be oxidized to acetone at 120 °C to yield a new vanadium(IV) hydrogen phosphate, $VO(HPO_4) \cdot 0.5H_2O$. Attempts to carry out this reaction on a larger scale in refluxing 2-propanol (bp 82.4 °C) failed because of the lower reaction temperature. However, refluxing a suspension of $VOPO_4 \cdot 2H_2O$ in 2-butanol (bp 98 °C) resulted in the production of the same blue vanadium hydrogen phosphate solid phase observed in the small scale experiments with 2-propanol at 120 °C along with 2-butanone as the organic oxidation product.

The yield of $VO(HPO_4) \cdot 0.5H_2O$ (see below) varies from 57% to 68%, with the remainder of the vanadium being transformed into a yellow, acetone-soluble V^{5+} compound. The amount of 2-butanone detected in the supernatant corresponds to the amount of solid isolated according to

$$2VOPO_4 \cdot 2H_2O + Et{-}CHOH{-}Me \rightarrow 2VO(HPO_4) \cdot 0.5H_2O + Et{-}CO{-}Me + 3H_2O$$

$VO(HPO_4) \cdot 0.5H_2O$ can be produced also by reaction of V_2O_5 with excess concentrated phosphoric acid in ethanolic solution. The ethanol serves to reduce the V^{5+} to V^{4+}, resulting in the production of acetaldehyde diethyl acetal. This preparation is more convenient because the need to prepare $VOPO_4 \cdot 2H_2O$ (from V_2O_5 and H_3PO_4) is eliminated and the yield is quantitative. The reaction in ethanol is slow but could probably be accelerated by replacing the ethanol with a higher boiling homologue. The synthesis from V_2O_5 is similar to those reported in the patent literature for the preparation of maleic anhydride catalyst precursors which employ isobutanol and solid H_3PO_4.[4,26,32] The product obtained by the H_3PO_4/EtOH method is blue-green while that produced by the $VOPO_4 \cdot 2H_2O$/2-butanol method is more blue, but their compositions as determined by elemental analysis, oxidation state titration, and infrared spectroscopy are identical. The powder X-ray diffraction patterns are also very similar, with the lines in the product produced by the V_2O_5/H_3PO_4/EtOH method being somewhat broader, indicating smaller crystallite size. The powder X-ray diffraction pattern and infrared spectrum demonstrate this to be the same compound reported as an "optimum" maleic anhydride catalyst precursor.[29,31]

The scanning electron micrographs shown in Figure 1 confirm the difference in crystallite size. The product formed by the $VOPO_4 \cdot 2H_2O$/2-butanol method is shown in Figure 1a. It is composed of well-formed plate-like crystals of approximate size 3×0.2 μm. The product from the V_2O_5/H_3PO_4/EtOH method has significantly smaller crystallites, less well-formed but still plate-like, with size on the order of 0.5×0.08 μm.

The vanadium hydrogen phosphate phase is formulated as $VO(HPO_4) \cdot 0.5H_2O$ on the basis of the combined evidence of elemental and thermogravimetric analysis, redox titrations, paper chromatography, and infrared spectroscopy. Elemental analyses give the stoichiometry $H_2VPO_{5.5}$ and redox titrations demonstrate the average vanadium valence to be 4.00. The infrared spectrum of $VO(HPO_4) \cdot 0.5H_2O$ and that of its fully deuterated analogue, prepared as described in the Experimental Section, are displayed in Figure 2. The bands for coordinated water at 3375 and 1642 cm^{-1} in the hydrogen compound are clearly distinguished. These bands shift to 2525 and ~1200 cm^{-1} after deuteration, though the lower frequency band in the deuterated compound is masked by the P–O stretching vibrations which occur in the 900–1200-cm^{-1} range. The infrared data demonstrate the presence of coordinated water in the compound. Comparison of the two spectra shows the absence of the 1132-cm^{-1} band of $VO(HPO_4) \cdot 0.5H_2O$ in its deuterated analogue and a slight shift to higher frequency (~10 cm^{-1}) of the 976-cm^{-1} band. Such changes would not be expected for a phosphate group that has no P–OH bonds, so they support the formulation of the compound as a hydrogen phosphate.

Paper chromatography can distinguish between orthophosphates and pyrophosphates or other more highly condensed phosphate anions. The results of paper chromatography experiments showed only orthophosphate was present in the compound.

The X-ray powder diffraction pattern of $VO(HPO_4) \cdot 0.5H_2O$ prepared by the $VOPO_4 \cdot 2H_2O$/2-butanol method is well resolved.

Figure 1. SEM photomicrographs of $VO(HPO_4) \cdot 0.5H_2O$ prepared by (a) the $VOPO_4 \cdot 2H_2O$/2-butanol method and (b) the V_2O_5/H_3PO_4/ethanol method. The bar in the lower right corresponds to 10 μm.

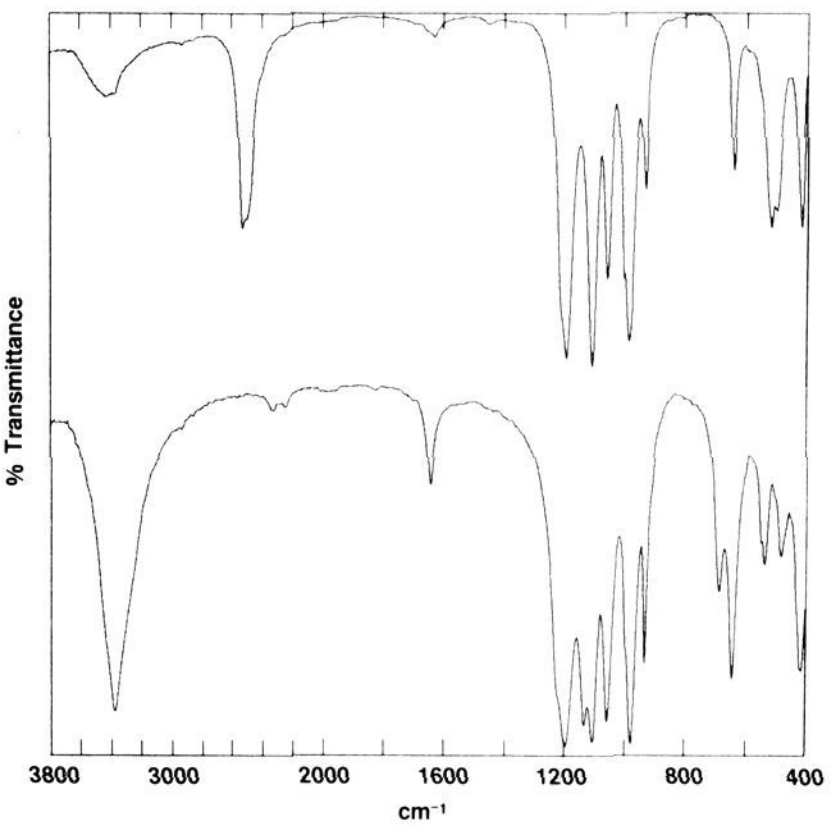

Figure 2. Infrared spectrum of $VO(HPO_4) \cdot 0.5H_2O$ (bottom) and its deuterated analogue (top).

The pattern was indexed in the orthorhombic crystal system with lattice constants $a = 7.434$ (2) Å, $b = 9.620$ (2) Å, and $c = 5.699$ (1) Å after least-squares refinement. The effects of preferred orientation on the 001 line show the c axis is normal to the major

Table I. X-ray Powder Diffraction Data for $VO(HPO_4)\cdot 0.5H_2O$[a]

hkl	d_{calcd}	d_{obsd}	$2\theta_{obsd}$	I_{obsd}
110	5.8823	5.901	15.00	2.9
001	5.6990	5.719	15.48	100.0
020	4.8100	4.818	18.40	2.0
101	4.5229	4.535	19.56	39.7
111	4.0931	4.099	21.66	5.0
021	3.6758	3.684	24.14	23.2
121	3.2950	3.300	27.00	32.2
201	3.1133	3.116	28.62	17.8
130	2.9444	2.944	30.34	34.6
220	2.9412			
031	2.7946	2.796	31.98	10.4
102	2.6607	2.663	33.62	26.7
131	2.6159	2.615	34.26	6.8
221	2.6136			
112	2.5645	2.567	34.92	5.1
022	2.4516	2.454	36.58	6.3
040	2.4050	2.405	37.36	3.7
310	2.3997			
202	2.2614	2.263	39.80	6.4
231	2.2337	2.234	40.34	4.9
311	2.2116	2.212	40.76	1.7
032	2.1300	2.131	42.38	4.6
321	2.0547	2.055	44.02	3.6
132	2.0476	2.047	44.20	5.9
222	2.0465			
330	1.9608	1.960	46.28	1.2
241	1.9033	1.903	47.74	7.1
013	1.8637	1.864	48.82	2.8
150	1.8626			
331	1.8541	1.854	49.10	9.0
312	1.8355	1.836	49.62	7.8
113	1.8077	1.808	50.44	1.5

[a] Orthorhombic; possible space groups *Pmmn* and $P2_1mn$; a = 7.434 (2) Å, b = 9.620 (2) Å, and c = 5.699 (1) Å; λ = 1.5405 Å.

platelet face. The data are presented in Table I. The systematic extinction for lines of the form *hk*0 when $h + k \neq 2n$ indicates that the possible space groups are *Pmmn* or $P2_1mn$. The detailed structure of $VO(HPO_4)\cdot 0.5H_2O$ was deduced from a single-crystal X-ray diffraction study[42] on a crystal grown from aqueous solution.

Magnetization (M) data were obtained from $VO(HPO_4)\cdot 0.5H_2O$ (prepared by the $VOPO_4\cdot 2H_2O$/2-butanol method) in applied magnetic fields (H) of 0–7.8 kG. $M(H)$ isotherms obtained at several temperatures were linear in H above 3 kG: $M(H,T) = M_s(T) + \chi_g(T)H$, where χ_g is the gram magnetic susceptibility and M_s is the saturation magnetization arising from ferromagnetic impurities. The values of M_s obtained were equivalent to the contribution of less than 20 molar ppm of ferromagnetic Fe metal impurities.

High-precision magnetic susceptibility data were obtained by measuring the magnetization in a fixed H of 6.35 kG upon sweeping the temperature at less than 1 K/min from 4 to 300 K. The data were corrected for the small contribution from ferromagnetic impurities and are plotted in Figure 3. With increasing temperature, χ_g first decreases rapidly but reaches a minimum at $T \sim 14$ K, increases monotonically up to 53 K, then smoothly decreases again with temperature up to 300 K, the maximum temperature of the measurement.

The inverse gram susceptibility is plotted vs. temperature in Figure 4. The data between 200 and 300 K are described very well by a Curie–Weiss behavior (cf. solid line in Figure 4): $\chi_g = C_g/(T - \theta)$, where $C_g = 2.08 \times 10^{-3}$ cm^3 K gm^{-1} is the gram Curie constant and $\theta = -25.3$ K is the Weiss temperature. The upward curvature of the data below ~200 K in Figure 4 is due to pairwise short-range antiferromagnetic ordering of the V^{4+} cations (see below), consistent with the negative sign of the Weiss temperature. The initial decrease in χ with increasing temperature from 4 to 14 K probably reflects the presence of isolated paramagnetic centers. The general features of the behavior of $\chi(T)$

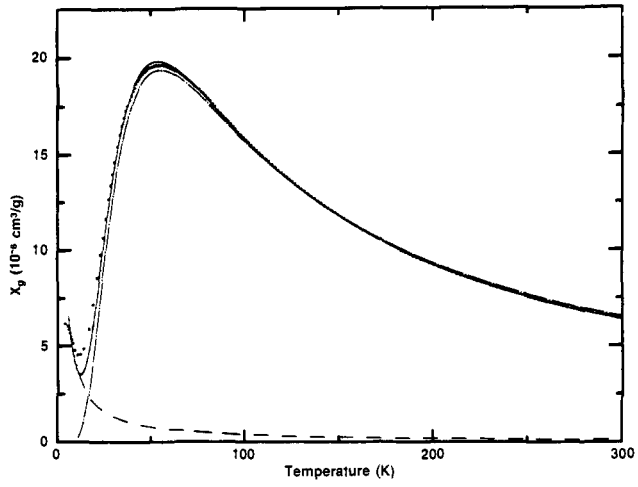

Figure 3. Gram magnetic susceptibility of $VO(HPO_4)\cdot 0.5H_2O$ vs. temperature.

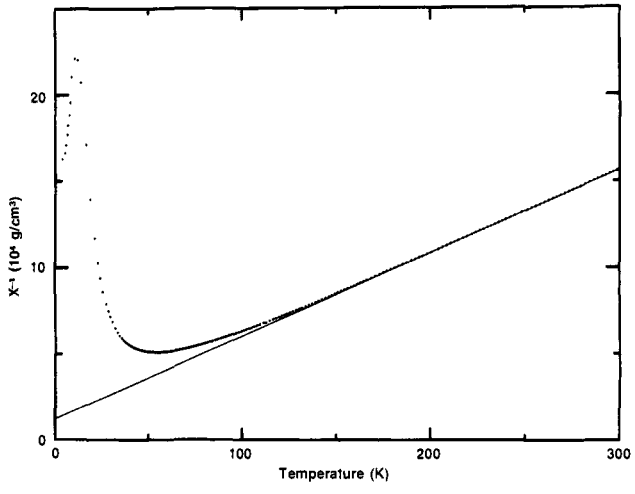

Figure 4. Inverse gram magnetic susceptibility of $VO(HPO_4)\cdot 0.5H_2O$ vs. temperature.

are also exhibited by molecular V^{4+} dimers.[43]

Thermal Reactions of $VO(HPO_4)\cdot 0.5H_2O$. $VO(HPO_4)\cdot 0.5H_2O$ retains its water of hydration tenaciously. The weight loss in inert atmosphere at a heating rate of 10 °C/min is displayed in Figure 5. The water is lost in one continuous step beginning at about 220 °C and with maximum slope at 450 °C. While most hydrated transition-metal salts lose coordinated water in the temperature range 100–200 °C, some layered vanadium oxide hydrates containing V^{4+} retain water of hydration up to 300 °C.[44]

A number of experiments were performed in which $VO(HPO_4)\cdot 0.5H_2O$ was heated in flowing He at temperatures varying from 400 to 800 °C. The results of these experiments are presented in Table II. In all cases, all lines in the X-ray powder diffraction patterns of the products could be indexed as those previously reported for vanadyl pyrophosphate, $(VO)_2P_2O_7$.[7] However, the crystallinity varied considerably, with samples prepared at lower temperatures showing fewer, broader, and weaker lines than samples prepared at higher temperatures. The color of the product varied from grey-brown to grey-green. Results of elemental analyses for vanadium and phosphorus agree well with the formula $(VO)_2P_2O_7$, particularly for the more crystalline samples. Table II lists the total weight loss observed upon heating to give $(VO)_2P_2O_7$. Values range between 11% and 12.5%, excluding a single experiment carried out at lower temperature in

(42) Leonowicz, M. E.; Johnson, J. W.; Brody, J. F.; Shannon, H.; Newsam, J. M. *J. Solid State Chem.*, in press.

(43) Ginsberg, A. P.; Koubek, E.; Williams, H. J. *Inorg. Chem.* **1969**, *5*, 1656–1662. Syamal, A. *Coord. Chem. Rev.* **1975**, *16*, 309–339.

(44) Aldebert, P.; Baffier, N.; Gharbi, N.; Livage, J. *Mater. Res. Bull.* **1981**, *16*, 669–676.

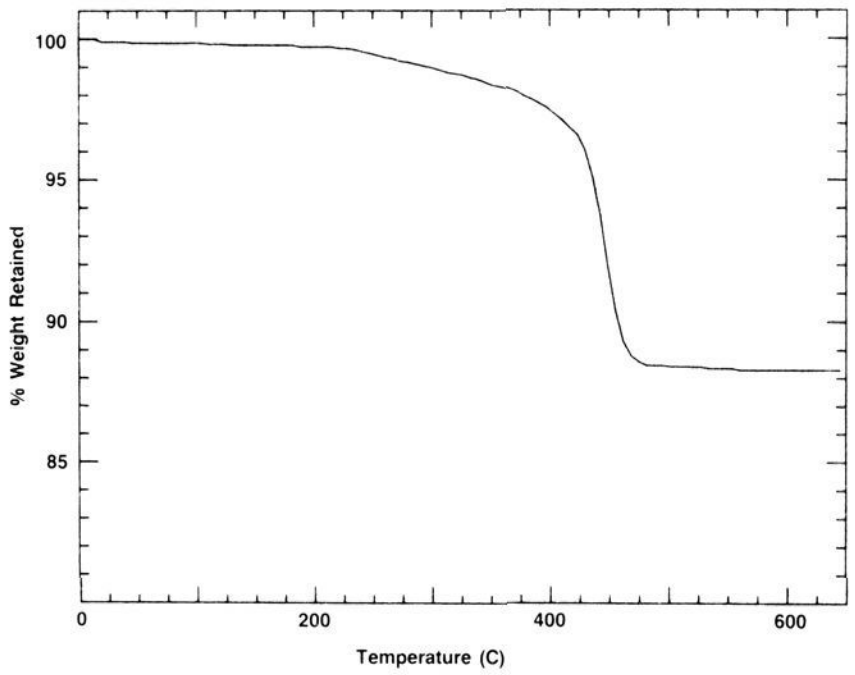

Figure 5. Thermogravimetric analysis of $VO(HPO_4)\cdot 0.5H_2O$ in flowing He at 10 °C/min.

Table II. Thermal Decomposition of $VO(HPO_4)\cdot 0.5H_2O$ in Flowing Helium

temp, °C	time	weight loss, %	crystallinity[a]
480[b]	16 h	11.10	1
412[c]	5 days	9.18	2
530[d]	3 days	12.09	2
610[b]	3 days	12.44	2
595	3 days	11.37	3
640[e]	5 days	11.46	3
755	4 days	11.53	4
780[b,f]	3 days	12.23	4

10.48% weight loss calculated for $VO(HPO_4)\cdot 0.5H_2O \rightarrow (VO)_2P_2O_7$

[a] Crystallinity qualitatively ranked by sharpness of $(VO)_2P_2O_7$ diffraction pattern (4 is most crystalline). [b] Prepared by $VOPO_4\cdot 2H_2O$/2-butanol method, other samples prepared by V_2O_5/H_3PO_4/EtOH method. [c] Atmosphere was He saturated with H_2O at room temperature. [d] Starting material was $VO(DPO_4)\cdot 0.5D_2O$. [e] Starting material was the product of (c); weight loss is cumulative. [f] Elemental analysis of product: 32.91% V, 20.58% P; calculated for $V_2P_2O_9$: 33.10% V, 20.12% P.

the presence of water vapor and also cooled to ambient temperature in water vapor.

The weight losses observed are slightly higher than the 10.48% expected for the reaction $2VO(HPO_4)\cdot 0.5H_2O \rightarrow (VO)_2P_2O_7 + 2H_2O$, possibly due to the presence of surface adsorbed water. The presence of structural water or O–H groups in the product is ruled out because the infrared spectrum of $(VO)_2P_2O_7$ prepared from $VO(HPO_4)\cdot 0.5H_2O$ (Figure 6) is identical with that of the material prepared from the fully deuterated analogue.

The dehydration reaction of $VO(HPO_4)\cdot 0.5H_2O$ to $(VO)_2P_2O_7$ occurs without altering the apparent size and shape of the individual crystallites as shown in Figure 7. In Figure 7a is a scanning electron micrograph of a sample prepared by the $VOPO_4\cdot 2H_2O$/2-butanol method and in Figure 7b the sample after it had been heated to ~500 °C for about 1 h. There is no gross change in crystallite size or morphology after the transformation from $VO(HPO_4)\cdot 0.5H_2O$ to $(VO)_2P_2O_7$.

When $VO(HPO_4)\cdot 5H_2O$ is heated in oxygen, the vanadium is oxidized from V^{4+} to V^{5+} during and after the loss of H_2O. A yellow compound of formula $VOPO_4$ is formed but its structure depends on the temperature of the reaction. Two new polymorphs, γ- and δ-$VOPO_4$ can be formed by control of the conditions. These will be described separately.

Discussion

The structure of $VO(HPO_4)\cdot 0.5H_2O$[42] is made up of vanadium octahedra and phosphorus tetrahedra with connectivity $VO(H_2O)_{1/2}O_{2/2}O_{2/3}P(OH)O_{2/2}O_{1/3}$ (Figure 8). The vanadium coordination sphere contains one multiply bound terminal oxygen

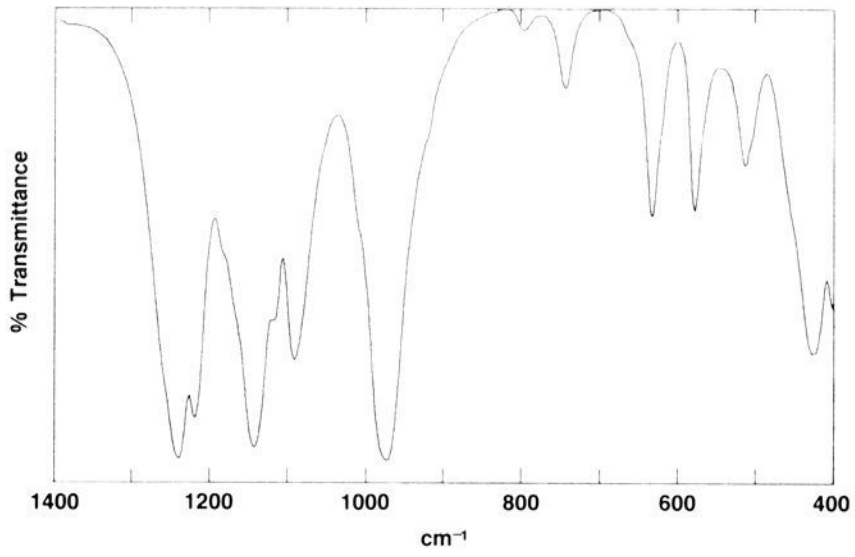

Figure 6. Infrared spectrum of $(VO)_2P_2O_7$.

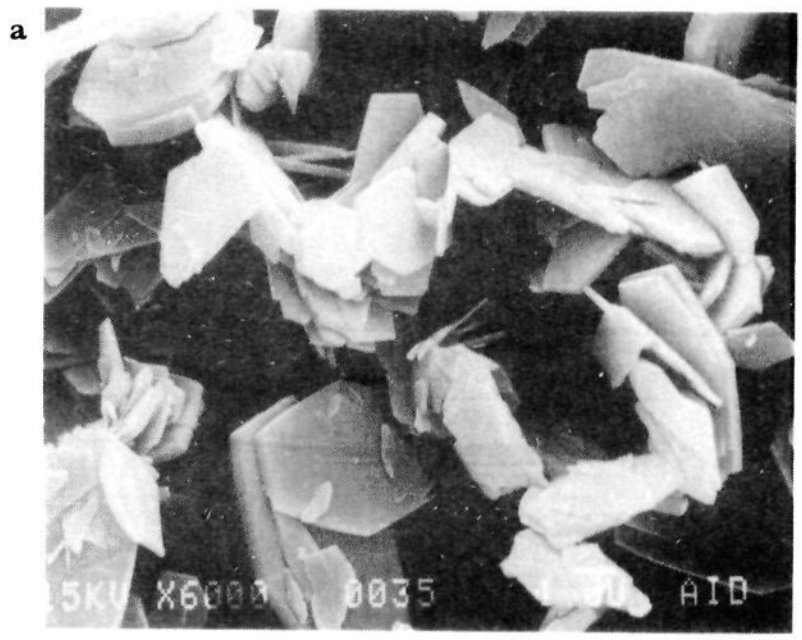

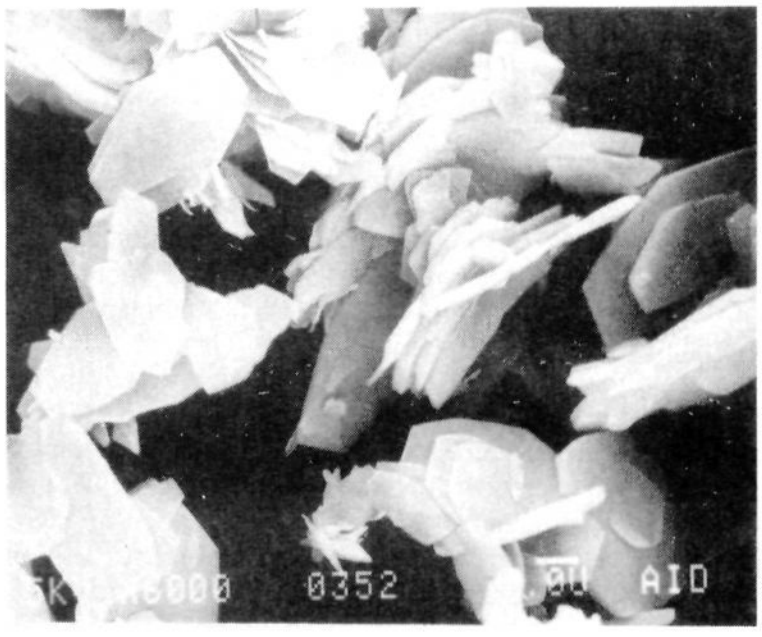

Figure 7. SEM photomicrographs of (a) $VO(HPO_4)\cdot 0.5H_2O$ and (b) $(VO)_2P_2O_7$ produced from it. The bar in the lower right corresponds to 1 μm.

(V=O) *trans* to a coordinated water molecule. The coordinated water molecule is shared between two nearest-neighbor vanadium atoms. The oxygens in the equatorial positions of the vanadium coordination sphere belong to HPO_4^{2-} groups. The phosphorus coordination sphere consists of an unshared -OH group directed toward the interlayer space, two oxygen atoms coordinated to a single vanadium, and one oxygen that is shared between two vanadium atoms. The layers are held together in the c direction through strong hydrogen bonding between the coordinated water molecules and the P–OH groups of adjacent layers. The strong hydrogen-bonded network is reflected in the high temperature required for water loss.

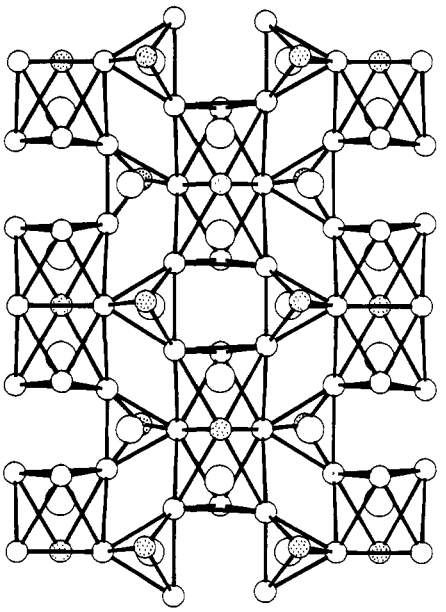

Figure 8. $VO(HPO_4)\cdot 0.5H_2O$ structure as viewed along *c*. Stippled atoms in the tetrahedra are hydroxyl oxygens and in the octahedra are water oxygens.

Table III. Parameters Used To Fit the Gram Magnetic Susceptibility Data for $VO(HPO_4)\cdot 0.5H_2O$

Curie–Weiss fit ($220 < T < 300$ K)	Bleaney–Bowers fit ($T < 300$ K, eq 1)
$C = 2.08 \times 10^{-3}$ cm^3 K g^{-1}	$\chi_0 = -3 \times 10^{-7}$ cm^3 g^{-1}
$\theta = -25.3$ K	$C^i = 4.0 \times 10^{-5}$ cm^3 K g^{-1}
	$C^d = 2.12 \times 10^{-3}$ cm^3 K g^{-1}
	$J = -30.6$ cm^{-1}
	$\mu_{eff} = 1.72\ \mu_B$

The interatomic distance between the V atoms in adjacent face-sharing octahedra within the *ab* plane of Figure 8 is 3.10 Å. In contrast, all other V–V distances within the *ab* plane are 4.87 Å or longer and the distance between the layers is 5.70 Å. The large difference between the nearest-neighbor and next-nearest-neighbor V–V distances suggest that the magnetic properties should exhibit behavior expected for isolated V_2 dimers. Assuming that the exchange coupling within a V_2 dimer is isotropic (i.e., the coupling energy is $-2JS_1S_2$), the magnetic susceptibility for an isolated dimer model containing two $S = {}^1/_2$ cations with isotropic *g* tensors is given by the Bleany–Bowers equation[46]

$$\chi = \chi_0 + \frac{C^i}{T} + \frac{4C^d}{T(3 + \exp(-2J/k_BT))} \qquad (1)$$

where χ_0 is a temperature-independent contribution, C^i/T is the Curie-like contribution from isolated paramagnetic centers, C^d is the Curie constant associated with the V_2 dimers, and k_B is Boltzmann's constant. In the limit of high temperatures ($|2J/k_BT| \ll 1$), the last term in eq 1 reduces to $\chi^d = C^d/(T - \theta)$, with $\theta = J/(2k_B)$, as observed in Figure 4. At low temperatures, $\chi^d \rightarrow 0$ and exhibits a broad maximum near $T \sim 2\theta$, as observed.

A quantitative fit of eq 1 to the data below 300 K was obtained for reasonable values of the adjustable parameters χ_0, C^i, C^d, and *J* (Table III) and is shown in Figure 3 (solid curve). The contributions of the V_2 dimers (dot-dashed curve) and the isolated spins (dashed curve) are also shown in Figure 3. If the isolated spins are assumed to be isolated V^{4+} defects, then the ratio of isolated to dimerized V^{4+} is $C^i/C^d = 1.9\%$ (cf. Table III). The sum of C^i and C^d is 2.16×10^{-3} cm^3 K gm^{-1}, close to the value of 2.08×10^{-3} cm^3 K gm^{-1} obtained above from the fit of the Curie–Weiss law to the high temperature data in Figure 4; the θ value (−22 K) derived from J ($\theta = J/(2k_B)$) is also close to that (−25.3 K) found from the Curie–Weiss fit. From $C^i + C^d$, one obtains the effective moment per V^{4+} ion $\mu_{eff} = 1.72\ \mu_B$, almost identical with the value 1.73 μ_B expected for a spin $^1/_2$ ion with $g = 2$. Finally, the (negative) value of χ_0 in Table III is close to the value computed for the diamagnetism of the ion cores (-3.4×10^7 cm^3/gm). To sum up, the susceptibility data are consistent with the structure of $VO(HPO_4)\cdot 0.5H_2O$ in which weakly exchange coupled ($J = -31$ cm^{-1}) vanadium dimers are effectively isolated from each other. The magnetic data are closely similar to previous results for several molecular VO^{2+} dimer systems in which *J* varies from −25 to −250 cm^{-1}.[43]

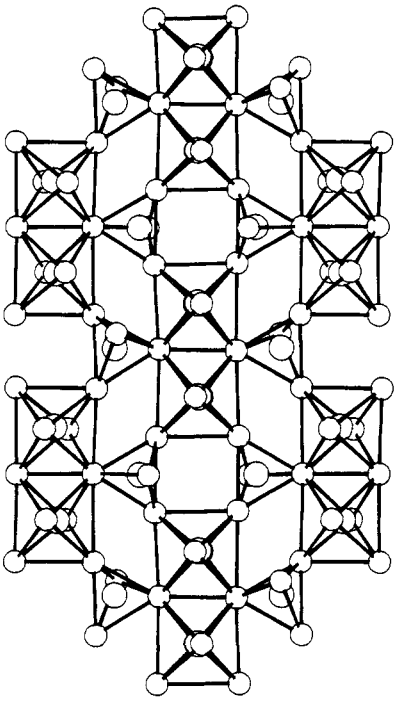

Figure 9. $(VO)_2P_2O_7$ structure as viewed along *a*.

The structure of the hemihydrate is closely related to that of $(VO)_2P_2O_7$. The structure of the pyrophosphate has previously been determined by single-crystal X-ray diffraction.[9] The unit cell is orthorhombic with lattice constants $a = 7.725$ Å, $b = 16.576$ Å, and $c = 9.573$ Å. A view of the structure looking down *a* onto the *bc* plane is shown in Figure 9. The layers are joined together through V—O═V and P—O—P bonds resulting in chains of vanadium octahedra sharing opposite corners and pyrophosphate ($P_2O_7^{4-}$) groups. The structure of $VO(HPO_4)\cdot 0.5H_2O$ in the *ab* plane is topologically similar to that of $(VO)_2P_2O_7$ in its *bc* plane (see Figures 8 and 9). The change from face-shared to edge-shared octahedra in converting the hemihydrate to the pyrophosphate results in a small expansion of one axis ($a = 7.434$ Å becomes $b/2 = 8.288$ Å) but the other in-plane dimension shows little change ($a = 9.620$ Å becomes $c = 9.573$ Å). The X-ray and scanning electron microscopy data suggest that the transformation is topotatic and occurs by condensation of the P–OH groups between adjacent layers and elimination of the coordinated water molecules. Transmission electron microscopy and electron diffraction confirm the proposed topotaxy of the dehydration reaction.[45]

Evidence for the formation of $VO(HPO_4)\cdot 0.5H_2O$ exists in the literature but the compound has not been thoroughly characterized. A maleic anhydride catalyst precursor prepared by an aqueous precipitation method[31] exhibits an X-ray powder diagram very similar to our data for $VO(HPO_4)\cdot 0.5H_2O$ (Table I). Recent patents[26b] use scanning electron microscopy to detail the morphology of catalysts prepared from V_2O_5 and H_3PO_4 in alcoholic medium. Finally, a recent publication reports both the IR and X-ray pattern of $VO(HPO_4)\cdot 0.5H_2O$ but misidentifies it as a

(45) Bordes, E.; Courtine, P.; Johnson, J. W. *J. Solid State Chem.* **1984**, *55*, 270–279.

(46) Bleaney, B.; Bowers, K. D. *Proc. R. Soc. London, Ser. A* **1952**, *A214*, 451–465.

pyrophosphate, $(VO)_2P_2O_7 \cdot 2H_2O$.[29]

The topotactic nature of the transformation from $VO(HPO_4) \cdot 0.5H_2O$ to $(VO)_2P_2O_7$, the active catalyst for the oxidation of butane to maleic anhydride, explains the crucial role of precursor morphology in determining catalyst performance which has been previously noted.[26] By synthesizing $VO(HPO_4) \cdot 0.5H_2O$ in alcoholic solvents under certain conditions,[26a] crystals with a plate-like morphology having the (001) face exposed are formed. The topotactic dehydration results in $(VO)_2P_2O_7$ with the (020) face of the resulting platelike crystallites being the major crystal face exposed.

Experimental Section

Unless otherwise noted, all procedures were carried out in air. Reagent grade V_2O_5, 85% H_3PO_4, and 95% EtOH were used as received. $VOPO_4 \cdot 2H_2O$ was prepared as described previously.[10,35] 2-Butanol (Aldrich, 99%) showed no 2-butanone by GLC analyses. Vanadium oxidation state measurements were performed by redox titrimetry, oxidizing the sample with a known excess of Ce^{4+}, and titrating the mixture with Fe^{2+} to determine unreacted Ce^{4+} and total V^{5+}. Powder X-ray diffraction patterns were measured on a Siemens D-500 automated diffractometer using monochromated Cu Kα radiation, with a 0.02° 2θ step every 5 s for an effective scan rate of 0.24° 2θ/min. An automatic routine subtracted Cu Kα_2 peaks and provided integrated intensities. Elemental analyses were performed by Galbraith Laboratories. FT-IR spectra, run in KBr pellets, and scanning electron micrographs were obtained from the ER&E Analytical and Information Division. Thermogravimetric analyses were done using either a Du Pont thermal analyzer, Models 951 and 990, or an evacuable Fisher 260F microbalance at a heating rate of 10 °C/min. GLC was done with a Hewlett-Packard 5840A with a Carbowax (10 ft., 10% on Chromasorb WHP) column at 90 °C and quantified by the standard addition method. Paper chromatography was performed as described in the literature.[47] Samples were dissolved in 0.02 M Na_4EDTA, as were standards of NaH_2PO_4 and $Na_4P_2O_7$. Orthophosphate gave an R_f value of 0.76, pyrophosphate gave 0.50. Only orthophosphate was observed in $VO(HPO_4) \cdot 0.5H_2O$. Magnetization measurements were carried out by using a modified George Associates Faraday Magnetometer equipped with a Perkin-Elmer AR-2 vacuum microbalance and a 4-in. Varian Electromagnet and constant current supply. The sample used for magnetic measurements was synthesized from highest purity commercially available starting materials. The accuracies of the reported temperatures and susceptibilities are ~1 K and ~1%, respectively.

Reaction of $VOPO_4 \cdot 2H_2O$ with 2-Butanol. $VOPO_4 \cdot 2H_2O$ (8.00 g, 0.0404 mol) was refluxed with stirring in 2-butanol (160 mL) for 21 h. After cooling, the resulting solid was filtered. 2-Butanone (0.010 g, 0.126 mol) was detected in the yellow filtrate. The solid was washed four times with acetone (50 mL). The initial washings were orange. The resulting light blue solid was dried in vacuo for 8 h to yield 4.74 g of $VO(HPO_4) \cdot 0.5H_2O$ (0.0276 mol, 68.2%). Anal. [Found (Calcd)]: 28.59% V (29.63), 18.19% P (18.02), 1.23% H (1.17).

Reaction of V_2O_5 with H_3PO_4 in Ethanol. V_2O_5 (15.00 g, 0.0825 mol) was refluxed with stirring in 95% EtOH (900 mL) containing H_3PO_4 (22.6 mL, 0.330 mol). During the reaction the suspension changed from orange to olive-green to pale blue-green. After 11 days, the solid was filtered from the clear supernatant, washed with acetone, and dried in vacuo for 16 h to yield 28.46 g of $VO(HPO_4) \cdot 0.5H_2O$ (0.166 mol, 100%). Anal. [Found (Calcd)]: 29.39% V (29.63), 17.79% P (18.02), 1.31% H (1.17).

Preparation of Deuterated Analogue. The reaction was set up in a flowing N_2 drybox to prevent H/D exchange with atmospheric moisture. The V_2O_5 and the glassware were oven-dried at 150 °C before use. V_2O_5 (0.300 g, 1.65 mmol) was placed in a 25-mL flask with ethanol-d_6 (99% D, 9.00 g), D_2O (0.50 g), and D_3PO_4 (85% in D_2O, 0.79 g, 6.65 mmol). The flask was fitted with a stirring bar and reflux condenser topped by a $CaSO_4$-filled drying tube and removed from the drybox. The mixture was refluxed with stirring for 11 days, cooled, and filtered. The resulting blue solid was washed with D_2O and dried at 60 °C in vacuo for 16 h to yield 0.567 g of $VO(DPO_4) \cdot 0.5D_2O$ (3.26 mmol, 98.8%).

Thermal Reactions of $VO(HPO_4) \cdot 0.5H_2O$. $VO(HPO_4) \cdot 0.5H_2O$ was placed in an alumina boat inside a silica tube in an electric furnace. Helium was passed through the tube while heating. The temperature inside the tube was monitored with a thermocouple placed immediately over the sample. The tube was purged overnight with helium before heating began. Samples were weighed before and after reaction on an analytical balance.

Acknowledgment. We thank H. J. Brady and J. A. Panella for TGA and M. E. Leonowicz for assistance in indexing the powder X-ray pattern of $VO(HPO_4) \cdot 0.5H_2O$. K. K. Rao, T. C. Yang, E. N. Suciu, and others of Exxon Chemical Company participated in helpful discussions concerning $VO(HPO_4) \cdot 0.5H_2O$ and its relation to maleic anhydride catalysts.

Note Added in Proof. The crystal structure of $VO(HPO_4) \cdot 0.5H_2O$ has recently been described.[48]

Registry No. $VOPO_4 \cdot 2H_2O$, 12359-27-2; $VO(HPO_4) \cdot 0.5H_2O$, 93280-40-1; $(VO)_2P_2O_7$, 58834-75-6; V_2O_5, 1314-62-1; 2-butanol, 78-92-2.

(47) Bernhard, D. N.; Chess, W. B. *Anal. Chem.* **1959**, *31*, 1026-1029.

(48) Torardi, C. C.; Calabrese, J. C. *Inorg. Chem.* **1984**, *23*, 1308-1310.

Dinuclear Elimination from Rhenium Hydrides and $AlMe_3$: Rhenium/Aluminum Polyhydrides

Wincenty A. Skupiński, John C. Huffman, Joseph W. Bruno, and Kenneth G. Caulton*

Contribution from the Department of Chemistry and Molecular Structure Center, Indiana University, Bloomington, Indiana 47405. *Received March 26, 1984*

Abstract: Reaction of Al_2Me_6 with ReH_7P_2 and with ReH_5P_3 (P = PMe_2Ph and $PMePh_2$) in benzene occurs with methane elimination to give $ReH_6AlMe_2P_2$ and $ReH_4AlMe_2P_3$, respectively. Each bimetallic compound is fluxional and shows evidence for both bridging and terminal hydride ligands. The X-ray crystal structure of $ReH_6AlMe_2(PMePh_2)_2$ shows it to be based on a ReH_6P_2 dodecahedron with $AlMe_2$ bound to two hydride ligands, forming a η^2-H_2AlMe_2 unit. Crystallographic data (−162 °C): triclinic, $P\bar{1}$ with $Z = 2$ and $a = 17.815$ (8) Å, $b = 10.386$ (4) Å, $c = 11.094$ (4) Å, $\alpha = 111.47$ (2)°, $\beta = 86.08$ (2)°, $\gamma = 95.78$ (2)°. The X-ray crystal structure of $ReH_4AlMe_2(PMePh_2)_3$ shows a ReH_4P_3 pentagonal bipyramid (one P axial and two equatorial) with $AlMe_2$ attached through *three* hydride ligands, one axial and two equatorial on Re, forming a $H_3AlMe_2^{2-}$ unit. Crystallographic data (−164 °C): monoclinic, $P2_1/a$ with $Z = 4$ and $a = 15.053$ (4) Å, $b = 15.900$ (4) Å, $c = 11.705$ (2) Å, and $\beta = 92.59$ (1)°. Evidence for the mechanism of these reactions is presented, and the trend for aluminum to achieve a coordination number greater than 4 is surveyed.

An open coordination site (i.e., a 16-valence electron configuration) is thought to be a prerequisite for binding a donor substrate to a metal complex. This being the case, we speculated that covalent attachment of an aluminum Lewis acid to a transition metal (eq 1) might provide a bimetallic complex with unsaturation at the main-group center which could provide a new means for

0002-7863/84/1506-8128$01.50/0